Progress In Electromagnetics Research, PIER 82, 109–125, 2008

ANALYSIS OF THE OPTICAL TRANSMISSION THROUGH THE METAL PLATE WITH SLIT ARRAY

Y. Fu, K. Li, and F. M. Kong

School of Information Science and Engineering
Shandong University
27 Shanda Nanlu, Jinan, 250100, China

Abstract—The near and far field properties of the large-scale metal plate with slit array are studied by applying the finite-difference time-domain (FDTD) method. The far region scattering properties at different incident angles are also discussed. We find out the enhanced optical transmission (EOT) through the metal plate with suitable placed narrow slit array is excited by the interaction of the surface plasmon polarization (SPP) and the Fabry-Perot resonance (FPR), and the dielectric substrate has significant influence on the transmission properties by affecting the electromagnetic field distribution on the metal-dielectric interface. Furthermore, the scattering field would be reduced and the transmission efficiency could be improved by the phase shift caused by the dielectric substrate. These unusual properties suggest possible applications to light-transparent metal contacts, stealth materials, etc.

1. INTRODUCTION

The extraordinary optical transmission (EOT) through sub-wavelength apertures on thin metallic films receives lots of attentions from scientists and engineers since Ebbesen *et al.* first reported this unusual phenomenon [1], and has been a rapid and expanding field of research [2–5]. Recently, the publication by Lalanne *et al.* [6] suggests that the EOT is caused by the surface plasmon polarization (SPP) and the Fabry-Perot resonance (FPR). The SPPs are electromagnetic surface waves that propagate along the metal-dielectric interface, and they are non-radiative [7]. Because the electromagnetic fields are localized and enhanced on the metal surface when the SPPs are excited, the SPPs have been widely applied in the sub-wavelength optics and plasmonics [8–13]. It is well known that the metal plates and films reflect and

absorb the emitting light in ordinary light-emitting diodes (LEDs), but a metal plate with narrow slit array can be light-transparent by the excitation of the EOT in some wavelength regions. Besides, a LED with the large-scale metal contact can make the current spreading uniform, has better heat dissipation performance to reduces the junction temperature of the current spreading layer and improve the internal quantum efficiency. These characteristics suggest possible application to a new type of LED based on the EOT.

In this paper, we theoretical study the EOT excitation condition, then the finite-difference time-domain (FDTD) [14] numerical method for the optical simulation is discussed, the far region data calculation method and the time domain iterative formulate for metal are described. In the discussion sections, the transmission properties of the slit array plate are studied by applying the FDTD method at first. Then the effects of GaP substrate to the transmission and scattering properties are studied. At last the near and far field properties of the structure at three typical EOT excitation conditions are discussed.

2. THE EOT EXCITATION CONDITION

When the incident light irradiates the metal plate with slits, light is transmitted through the plate along the sub-wavelength slits. Then the light is scattered from the metal corners and part of the light propagates along the metal-air interface, which is a creeping wave. If the propagation constant of the creeping wave (k_{sp}) satisfies the resonance condition, enhanced electromagnetic fields are excited, and the light is radiated to the far region by the interaction of the guiding wave (k_r) and the creeping wave (k_{sp}) (Fig. 1).

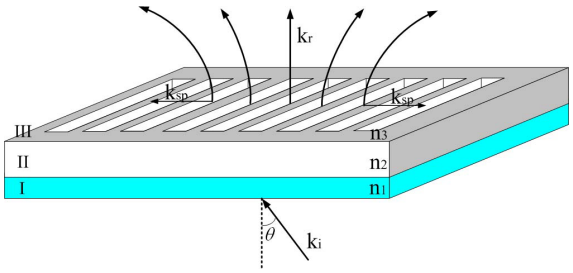

Figure 1. The schematic diagram of the EOT excitation. Region I is the dielectric layer, region II is the silver plate with slit array, and region III is the free space. The reflective index of GaP $n_1 = 3.2$, the reflective index of Silver at 610 nm is $n_2 = 0.268 + i4.109$, and the reflective index of air is $n_3 = 1.0$.

It is can be seen that the EOT condition is defined by two parameters, the thickness of the metal plate and the period of the slit array. The transmission efficiency through the plate reaches maximum when the slit thickness matches the FPR condition:

$$\frac{m\lambda}{n_{eff}} = 2(h - 2\sigma) \quad (m = 1, 2, ...), \tag{1}$$

where h is the slit thickness, λ is the free-space wavelength, the skin depth is $\sigma = 1/Im\left(\omega\sqrt{\mu\epsilon_m}\right)$ [15], and n_{eff} is the effective index, which is a function of the propagation constant,

$$n_{eff} = Re\left(\frac{k_r}{k_0}\right), \tag{2}$$

where Re denotes the real part, the free-space propagation constant is $k_0 = 2\pi/\lambda$, and k_r is the propagation constant in the slit. k_r could be calculated by the following equation,

$$k_r = \sqrt{\omega^2\mu\epsilon - \left(n\frac{\pi}{a}\right)^2 - k_{sp}^2} \quad (n = 0, 1, 2, ...), \tag{3}$$

where k_{sp} is the propagation constant along the lower metal-dielectric interface. The strong coupling is excited when k_{sp} satisfies following condition,

$$k_{sp} = k_x \pm l\frac{\pi}{p} \quad (l = 0, 1, 2, ...), \tag{4}$$

where k_x is the transverse component of the incident wave vector (i.e. k_ir in Fig. 1), and p is the period of the slit array. $k_x = 0$ at the normal incident condition, so Eq. (4) is simplified to

$$k_{sp} = \pm l\frac{\pi}{p} \quad (l = 0, 1, 2, ...). \tag{5}$$

when l is an even number, Eq. (5) is the SPP condition [1]. By now, the equations for the EOT wavelength calculation are obtained. For the intuitive expression a variable φ is introduced, and Eq. (1) is modified to the following form,

$$\varphi = \frac{2\pi(h - 2\sigma)n_{eff}}{\lambda}. \tag{6}$$

When $\varphi = m\pi$, the FPR condition is satisfied. We substitute Eqs. (2), (3), and (5) into Eq. (6) and get the following equation:

$$\varphi = \frac{2\pi\left(h - \dfrac{2}{Im(\omega\sqrt{\mu\epsilon_m})}\right) \times Re\left(\sqrt{v_c^2\mu\epsilon - \left(n\dfrac{\lambda}{2a}\right)^2 - \left(l\dfrac{\lambda}{2p}\right)^2}\right)}{\lambda} \quad (l = 0, 1, 2, ...; n = 0, 1, 2, ...). \quad (7)$$

3. THE FDTD METHOD

The FDTD method is a time-domain computational method based on the Maxwell's equations. It is a powerful technique for analyzing electromagnetic problems, and has been widely used in electromagnetic and optical simulations [16–22]. In the following FDTD simulations, TM plane waves T_{inc}, where T denotes E and H, are generated on the total field (TF)-scattered field (SF) boundary (Fig. 2) [23]. The fields in the total region are calculated as $T_{tot} = T_{inc} + T_{scat}$, i.e., the sum of the incident fields and the scattered fields, and there are only scattered fields T_{scat} in the scattered region. The near field properties are got by calculating the maximum field amplitudes and the respect phases ϕ of each points, which are calculated by

$$\phi = 2\pi\left(-\frac{v_c}{\lambda}k\Delta t + \frac{1}{4}\right), \quad (8)$$

after the calculation domain is stable during the simulation. The far region data can not be calculated from the simulation directly as the simulation domain is finite. In order to get the far field properties, the Kirchhoff surface is introduced, the electromagnetic fields are defined to zero inside the surface, and the problem becomes a radiation problem of the electric current and magnetic current on the surface. The electric current $\vec{J}$ and magnetic current $\vec{J_m}$ are calculated by the electromagnetic fields on the surface:

$$\begin{cases} \vec{J} = \vec{e_n} \times \vec{H} \\ \vec{J_m} = -\vec{e_n} \times \vec{E} \end{cases} \quad (9)$$

Then the far region data can be calculated by applying the Green function [24–27]. The parameters in the simulations are as follows: the mash size is $\Delta s = 5\,\text{nm}$, the time step is $\Delta t = \Delta s/2c$, the total time step is 20000. The perfectly matched layer (PML) [28] and Bloch's periodic boundary condition (BPC) are applied to the absorbing boundaries.

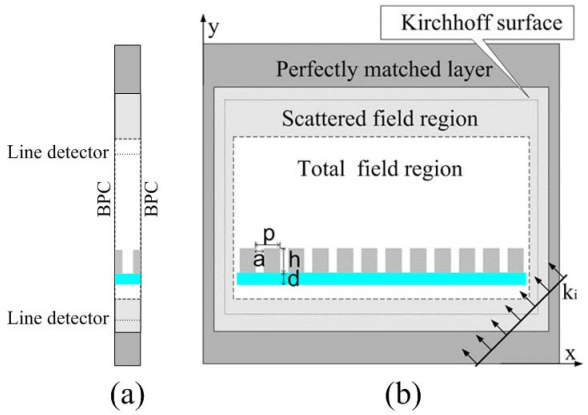

Figure 2. The layout of the FDTD simulation domain. (a) is the layout for the transmission and reflection spectrum calculation, the calculation space is 610 nm$\times 4\mu$m. (b) is the layout for the the near and far field property calculation, the calculation space is $7.5\,\mu\text{m} \times 4\,\mu\text{m}$. The slit array period is $p = 610\,\text{nm}$, the slit width is $a = 200\,\text{nm}$, the silver plate thickness is $h = 610\,\text{nm}$, and the GaP thickness is $d = 300\,\text{nm}$. In layout (b), the silver plate width is $7.1\,\mu\text{m}$ and the slit number is 11.

The modeling of the metal is a key step in the optical FDTD simulation. Traditional FDTD analysis for metal is not suitable for the analysis of nanoscale optics because the metallic structure has the same scale with the skin depth. The drude model has been introduced to approximate the dielectric constant of metal:

$$\epsilon = \epsilon_\infty - \frac{\omega_p^2}{(\omega^2 + j\omega\gamma)}, \tag{10}$$

where ϵ_∞ is the relative permittivity at infinite frequency, ω_p is the plasma angle frequency and γ is the collision angle frequency. The parameters of silver ($\epsilon_\infty = 5.0$, $\omega_p = 9.5\,\text{eV}$, and $\gamma = 0.0987\,\text{eV}$) is accordance with the experimental data in optical and infrared regions [29]. The time domain iterative formulate are calculated by the frequency-dependent FDTD ((FD)^{2}TD) [30] method,

$$E_\varsigma^{n+1}(i,j) = \frac{\epsilon_\infty + \Delta\chi_0}{\epsilon_\infty + \chi_0} E_\varsigma^n(i,j) + \frac{1}{\epsilon_\infty + \chi_0} \Psi_\varsigma^n(i,j) + \frac{\Delta t}{(\epsilon_\infty + \chi_0)\,\epsilon_0 \Delta s} \frac{\partial H_z^{n+\frac{1}{2}}(i,j)}{\partial \varsigma}, \tag{11}$$

$$\Psi_\varsigma^{n+1}(i,j) = e^{-\gamma \Delta t} \Psi_\varsigma^n(i,j) + \Delta\chi_1 E_\varsigma^{n-1}(i,j). \tag{12}$$

where

$$\Delta\chi_0 = -\left(\frac{\omega_p}{v_c}\right)^2 \left[1 - e^{-v_c \Delta t}\right]^2, \tag{13}$$

$$\chi_0 = \frac{\omega_p^2}{v_c}\Delta t - \left(\frac{\omega_p}{v_c}\right)^2 \left[1 - e^{-v_c \Delta t}\right], \tag{14}$$

$$\Delta\chi_1 = -\left(\frac{\omega_p}{v_c}\right)^2 e^{-v_c \Delta t} \left[1 - e^{-v_c \Delta t}\right]^2, \tag{15}$$

and $\varsigma = x, y$, v_c is the light speed. The magnetic field iterative formulate are same with that of dielectric. In order to improve the calculation speed and simplify programming, a two-dimensional array is introduced to store the material type of each point. The calculations in this paper were performed on a 2.8 GHz Pentium (R) D computer. The calculation time cost is 320 seconds and the memory cost is 47 MB for the spectrum calculation. The time cost is 54 minutes and the memory cost is 130MB for the near and far field property calculation.

4. RESULTS AND DISCUSSION

The optical property of the infinite slit array at the normal incident condition is studied at first. The phase-wavelength curve calculated by Eq. (7) is shown in Fig. 3. From Fig. 3 it is observed that the longest EOT wavelength is 826.5 nm (i.e., point A in Fig. 3), and the parameters are $n = 0$, $\phi = 0$, and $\theta = \pi$, which means that only the FPR is excited ($\theta = \pi$) and no creeping wave coupling is excited ($\phi = 0$). The second EOT case corresponds to point B, the wavelength is 610 nm. The parameters are $n = 0$, $\phi = 2\pi$, and $\theta = 0$, which means that only the SPP is excited ($\phi = 2\pi$) and no FPR is excited ($\theta = 0$). The other EOT wavelengths (C, D, E, and F) meet both the creeping wave coupling condition and the FPR condition. When the wavelength is shorter than 400 nm (i.e., the gray region in Fig. 3), the curves are sharp and the phase changes quickly, hybrid modes with different EOT excitation conditions would interact and cancel each other. In order

to verify the results, the FDTD method is employed. The layout is shown in Fig. 2(a). The source is a Gaussian pulse, and field values on detector lines are stored in the simulation. The transmission and reflection spectrum are calculated by applying fast fourier transform (FFT), and the spectra are shown in Fig. 4. It can be seen that the result is in accord with our calculation. The field distributions at

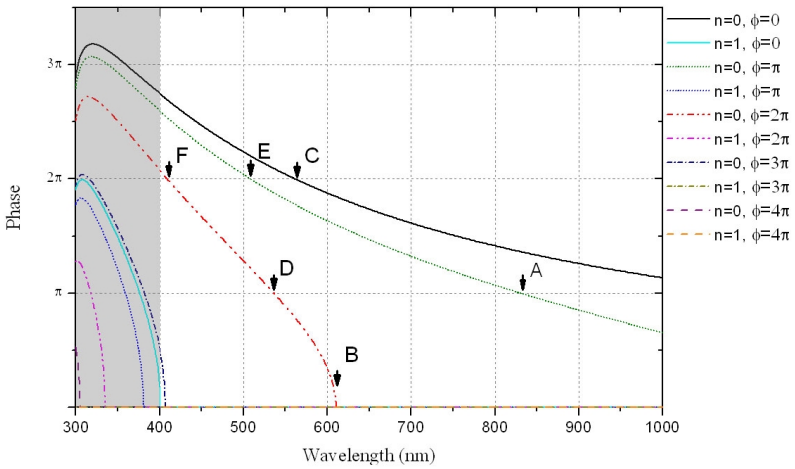

Figure 3. The phase-wavelength curve. The EOT wavelengths are marked by the arrows, and $\phi = l\pi$.

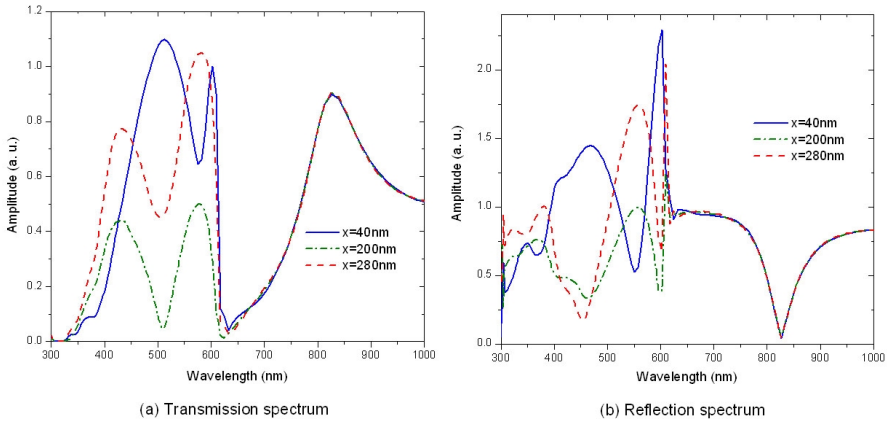

Figure 4. The transmission and reflection spectra of the silt array silver plate. (a) is the transmission spectrum on the line of $y = 3.875\,\mu$m and (b) is the reflection spectrum on the line of $y = 50\,$nm.

different points are same when the wavelength is longer than the SPP wavelength (i.e., 610 nm), for resonance is excited on neither upper nor lower silver-dielectric interface. Energy is mainly forward transmitted at the FPR wavelength (i.e., 826.5 nm). When the wavelength is close to the SPP wavelength, both transmission and reflection are enhanced, and the curves are precipitous. When the wavelength is shorter than the SPP wavelength, the field distributions at different points are different because of the resonance and interference. And the transmission spectrum curve has a peak point at the wavelength of 510 nm. In short, the EOT is caused by two different mechanisms: the creeping wave coupling and the FPR. This is in agreement with our discussion in Section 2. The FPR plays the key role in the long wavelength region, the interference of the creeping waves and the guiding waves becomes the main factor that excites the EOT in the short wavelength region.

The optical properties of the slit array plate have been discussed, however, in the photoelectric fabrication, the metal is usually placed on dielectric substrates, and GaP is widely used as the LED current spreading layer. The studies on the effects of the GaP substrate to the structure have practical significance. For the dielectric constant of GaP is 11.1, the propagation constant is much smaller than that in free space, and the transmission properties of the structure would be different. The transmission and reflection properties of the slit array plate with GaP substrate are calculated in the same way. The

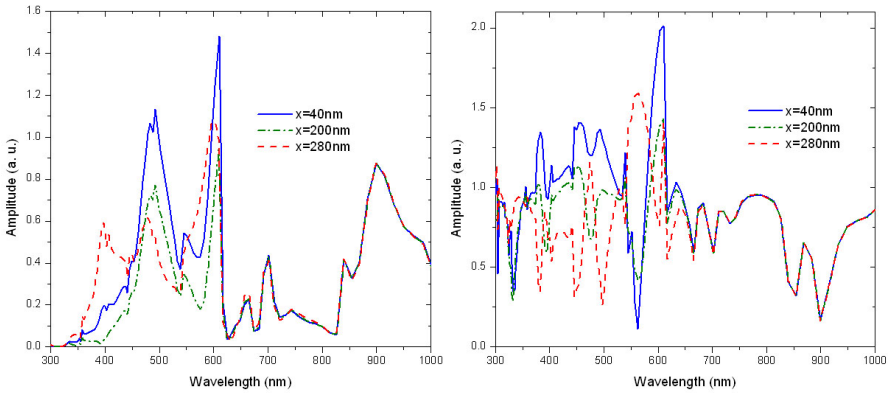

Figure 5. The transmission and reflection spectra of the silt array silver plate with GaP substrate. (a) is the transmission spectrum on the line of $y = 3.875\,\mu$m and (b) is the reflection spectrum on the line of $y = 50$ nm.

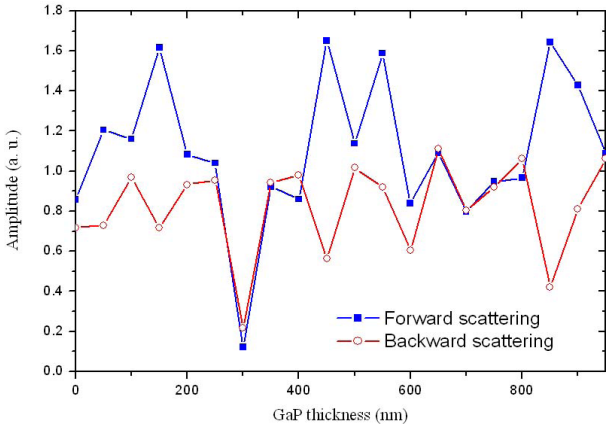

Figure 6. The forward and backward scattering magnetic intensity with different substrate thickness. The source wavelength is 900 nm.

spectrum curves as seen in Fig. 5, are much sharper than that without GaP substrate, and the curve shapes are more complex. Furthermore, the Amplitude of Hz component is 50% stronger than that without GaP substrate at the SPP wavelength. It can be seen that the GaP substrate affects the transmission properties greatly. We believe that the enhancement is caused by the changing of the field distribution and the phase shift by the EM waves at the lower interface of the Ag-GaP layers. Moreover, because of the phase shift caused by the GaP substrate, a suitable GaP substrate thickness can module the phase of the scattered wave T_{scat} with the incident wave T_{inc}, and make the structure be a light-transparent meta-material. The scattering features of the structure at the FPR wavelength (i.e., 900 nm) are studied. A set of GaP substrate thickness from 0 nm to 950 nm with the step 50 nm are simulated. The forward and backward scattering curves are shown in Fig. 6. It can be seen that when the GaP thickness is equal to 300 nm, rarely light is scattered: the forward scattering magnetic intensity is only 0.1 $a.u.$ and the backward scattering magnetic intensity is 0.2 $a.u.$. This unique light-transparent characteristic suggests possible applications on LEDs, stealth technology, etc. The near and far field properties on this situation are studied in detail in the following section.

4.1. EOT Excited by the FPR

The layout of simulation is same with that in Fig. 2(b). The magnetic field distribution is shown in Fig. 7(a). As seen in Fig. 7, the light

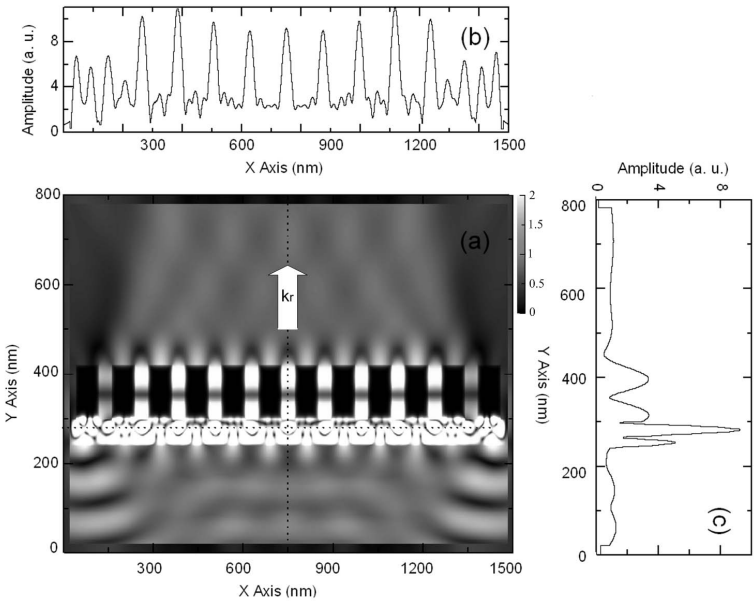

Figure 7. The near field distribution of the silver plate with the source wavelength of 900 nm. (a) is the intensity of the Hz component, (b) is the magnetic intensities on the line of $y = 280$ nm, and (c) is the magnetic intensities on the line of $x = 750$ nm.

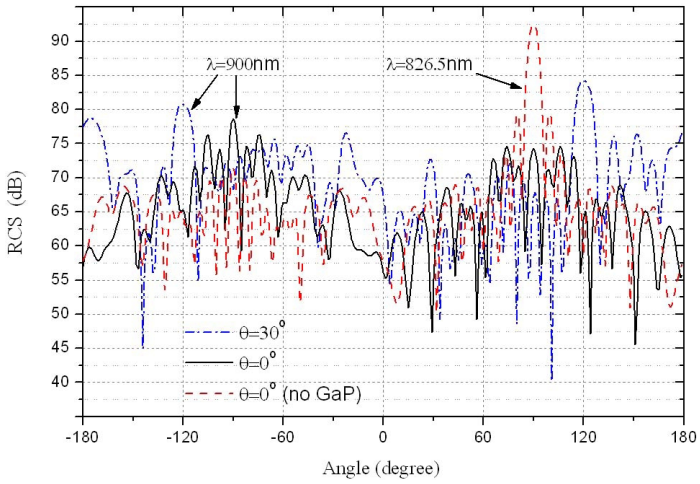

Figure 8. The far region scattering curves at the FPR condition.

is resonance enhanced in the slits, and each slit is equivalent to a new point source on the upper side. the creeping wave component can not propagates for the wavelength is much longer than the slit interval, it means that the propagating constant is equal to zero along the x axis, so the light is radiated to the far region, and the wave vector direction is along the y axis. The curves in the Fig. 7(c) shows that the transmission efficiency through the Ag plate is almost 90%. The magnetic distribution in the GaP substrate, which is displayed in Fig. 7(b), is enhanced and localized.

The far region scattering properties are also discussed (Fig. 8). The solid line is the far region scattering curve at the normal incident, and the dash line is the scattering curve of the structure without GaP substrate. It is denotes that the light is strongly forward scattered by the structure without GaP, the reflection is 20 dB lower than the forward scattering. The GaP substrate cancels the scattering, the maximum scattering is 15 dB lower than the forward scattering of the structure without GaP substrate. The performance reduces quickly with the increase of the incident angle for the FPR in the slits is attenuated and light is absorbed and reflected by the silver plane. The dash-dot line is the scattering curve at 30° oblique incident, the forward scattering is 8.5 dB lower than that at the normal incident, meanwhile the backward scattering is increased by 2 dB. In short, the EOT excited by the FPR is angle-sensitive, large incident angles would decrease the forward transmission performance greatly.

4.2. EOT Excited by the SPP

The SPP is excited on the upper interface of Ag-air at this excitation condition, light is coupling to the transverse component k_{sp}, and the wave vector direction is along the x axis. The near field distribution as shown in Fig. 9 represents that the magnetic intensity is strongest in the center, and the intensity reduces with the increase of the distance from the center as the coupling strength reduces. In addition, the field amplitude (i.e., about 100 nm) is much larger than the ordinary SPP amplitude because of the interference of the creeping wave and the transmitted light from the slits. The field distribution is much complex in the GaP substrate, the SPPs are excited on the lower Ag-GaP interface (Fig. 9 (b)), and no significant enhancement occurs at the slit entry. The far region scattering curves, which are shown in Fig. 10, denote that the structure is less angle-sensitive. The forward scattering strength is the same with that at normal incident even the incident angle is increased to 30°. This characteristic could be explained for the reason that the EOT is mainly caused by the coupling of the creeping waves on the upper Ag-air interface. With the continue increase of

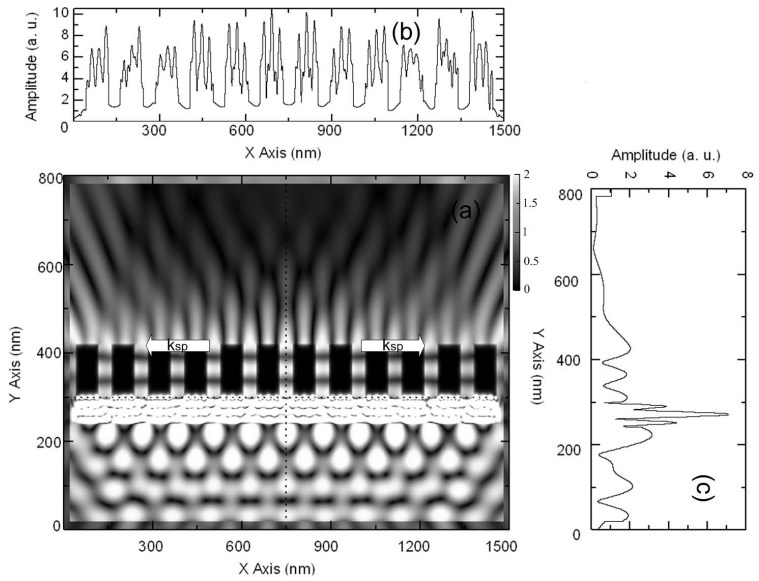

Figure 9. The near field distribution of the silver plate with the source wavelength of 900 nm. (a) is the intensity of the Hz component, (b) is the magnetic intensities on the lower interface (i.e., $y = 300$ nm), and (c) is the magnetic intensities on the line of $x = 750$ nm.

the incident angle, less light is transmitted through the plate, when the incident angle is equal to 60°, the transmission efficiency reduces greatly for the reflection and the absorption on slits and the silver-GaP interface.

4.3. EOT Excited by the Creeping Wave Coupling and FPR

The last EOT case is the interference of the guiding waves from the slits and the strong coupling creeping waves on the silver plate surface. This excitation condition is more common and has better performance because that the EOT is excited by the interference of the strong coupling creeping waves and the FPR, the enhanced EM waves are radiated to the space for the enhancement in the interface is excited by the creeping waves, which is radiative, not like the non-radiative SPP. The near field distribution is shown in Fig. 11, the magnetic fields are enhanced both on the slits and the Ag plate positions in the GaP substrate (Fig. 11(b)), and the light is enhanced on the upper side of the slit and Ag plate (Fig. 11(c)). Then the light is radiated to the free

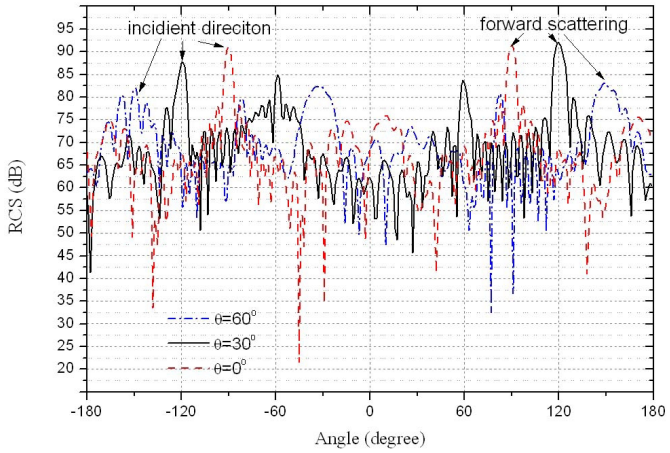

Figure 10. The far region scattering curves at the SPP condition. The source wavelength is 610 nm.

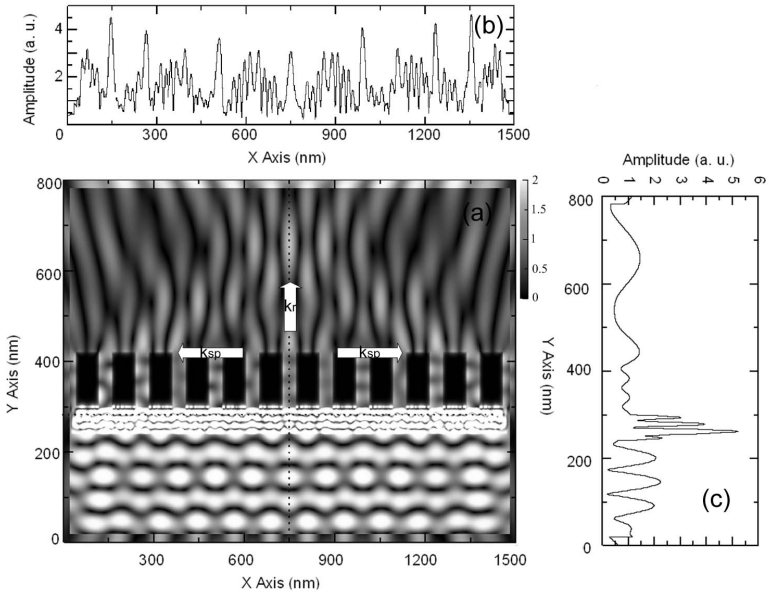

Figure 11. The near field distribution of the silver plate with the source wavelength of 900 nm. (a) is the intensity of the Hz component, (b) is the magnetic intensities on the line of $y = 285$ nm, and (c) is the magnetic intensities on the line of $x = 750$ nm.

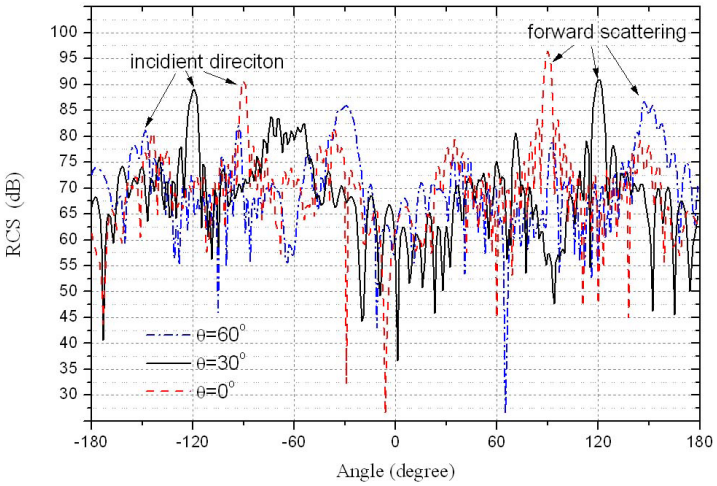

Figure 12. The far region scattering curves with the source wavelength of 500 nm.

space by the interference of the creeping waves and the guiding waves. The wave vector is the combination of the x-direction component and the y-direction component. The far region scattering properties in Fig. 12 shows that this EOT case has the strongest scattering field and is not angle-sensitive.

5. CONCLUSION

In conclusion, we have theoretical analyzed the EOT condition of the metal plate with sub-wavelength slit array, and modeled the FDTD model for metal. The near and far field properties of the large-scale silver plate with slit array are numerically analyzed. And three typical EOT conditions are studied. The effects of the dielectric substrate are also discussed. We find out that the metallic structure could be light-transparent, and the EOT would be excited when the geometry of the structure matches the resonance enhancement conditions. Moreover, the dielectric substrate has significant influence on the transmission properties by affecting the field distribution on the metal-dielectric interface, improves the transmission efficiency and reduces the scattering by the phase shift at resonance wavelengths of the structure. These unusual properties suggest possible applications to light-transparent metal contacts, stealth materials, etc.

ACKNOWLEDGMENT

This work is supported by the Key Project of Chinese Ministry of Education (No. 105101) and Natural Science Foundation of Shandong Province (No. 31170005200605).

REFERENCES

1. Ebbesen, T. W., H. J. Lezec, H. F. Ghaemi, T. Thio, and P. A. Wolff, "Extraordinary optical transmission through sub-wavelength hole arrays," *Nature*, Vol. 391, No. 6668, 667–669, 1998.
2. Genet, C. and T. W. Ebbesen, "Light in tiny holes," *Nature*, Vol. 445, No. 7123, 39–46, 2007.
3. Beruete, M., M. Sorolla, and I. Campillo, "Left-handed extraordinary optical transmission through a photonic crystal of sub-wavelength hole arrays," *Opt. Express*, Vol. 14, No. 12, 5445–5455, 2006.
4. Mary, A., S. G. Rodrigo, L. Martin-Moreno, and F. J. Garcia-Vidal, "Theory of light transmission through an array of rectangular holes," *Physical Review B*, Vol. 76, No. 19, 195414, 2007.
5. Ghazi, G. and M. Shahabadi, "Modal analysis of extraordinary transmission through an array of subwavelength slits," *Progress In Electromagnetics Research*, PIER 79, 59–74, 2008.
6. Lalanne, P. and J. P. Hugonin, "Interaction between optical nano-objects at metallo-dielectric interfaces," *Nature Phys.*, Vol. 2, No. 8, 551–556, 2006.
7. Raether, H., *Surface Plasmons on Smooth and Rough Surfaces and on Gratings*, Spring-Verlag, Berlin, 1988.
8. Ozbay, E., "Plasmonics: Merging photonics and electronics at nanoscale dimensions," *Science*, Vol. 311, No. 5758, 189–193, 2006.
9. Suyama, T. and Y. Okuno, "Enhancement of TM-TE mode conversion caused by excitation of surface plasmons on a metal grating and its application for refractive index measurement," *Progress In Electromagnetics Research*, PIER 72, 91–103, 2007.
10. Lin, L., R. J. Blaikie, and R. J. Reeves, "Surface-plasmon enhanced optical transmission through planar metal films," *Journal of Electromagnetic Waves and Applications*, Vol. 19, No. 13, 1721–1728, 2005.
11. Kong, F. M., K. Li, B. I. Wu, H. Huang, H. Chen, and J. A. Kong,

"Propagation properties of the SPP nano scale narrow metallic gap, channel, and hole geometries," *Progress In Electromagnetics Research*, Vol. 76, 449–466, 2007.

12. Liaw, J. W., M. K. Kuo, and C. N. Liao, "Plasmon resonances of spherical and ellipsoidal nanoparticles," *Journal of Electromagnetic Waves and Applications*, Vol. 19, No. 13, 1787–1794, 2005.
13. Talele, K. and D. S. Patil, "Analysis of wave function, energy and transmission coefficients in Gan/Algan superlattice nanostructures," *Progress In Electromagnetics Research*, PIER 81, 237–252, 2008.
14. Yee, K., "Numerical solution of inital boundary value problems involving maxwell's equations in isotropic media," *IEEE Trans. Antennas Propagat.*, Vol. 14, No. 3, 302–307, 1966.
15. Kong, J. A., *Electromagnetic Wave Theory*, Wiley & Sons, New York, 1986.
16. Kuzu, L., V. Demir, A. Z. Elsherbeni, and E. Arvas, "Electromagnetic scattering from arbitrarily shaped chiral objects using the finite difference frequency domain method," *Progress In Electromagnetics Research*, Vol. 67, 1–4, 2007.
17. Oubre, C. and P. Nordlander, "Optical properties of metallodielectric nanostructures calculated using the finite difference time domain method," *J. Phys. Chem. B*, Vol. 108, No. 46, 17740–17747, 2004.
18. Ali, M. and S. Sanyal, "FDTD analysis of dipole antenna as EMI sensor," *Progress In Electromagnetics Research*, Vol. 67, 341–359, 2007.
19. Zhao, Y., P. Belov, and Y. Hao, "Accurate modeling of the optical properties of left-handed media using a finite-difference time-domain method," *Phys. Rev. E*, Vol. 75, No. 3, 37602–37605, 2007.
20. Wang, M. Y., J. Xu, J. Wu, Y. Yan, and H. L. Li, "FDTD study on scattering of metallic column covered by double-negative metamaterial," *Journal of Electromagnetic Wave Applications*, Vol. 21, No. 12, 1905–1914, 2007.
21. Hu, X. J. and D. B. Ge, "Study on conformal FDTD for electromagnetic scattering by targets with thin coating," *Progress In Electromagnetics Research*, PIER 79, 305–319, 2008.
22. Afrooz, K., A. Abdipour, A. Tavakoli, and M. Movahhedi, "Time domain analysis of active transmission line using FDTD technique (application to cicrowave/mm-wave transistors)," *Progress In*

Electromagnetics Research, PIER 77, 309–328, 2007.

23. Taflove, A. and S. C. Hagness, *Computational Electrodynamics: The finite-difference time-domain method*, 2nd edition, Artech House, Boston, 2000.
24. Ramahi, O. M., "Near-and far-field calculations in FDTD simulations using Kirchhoff surface integral representation," *IEEE Trans. Antennas Propagat.*, Vol. 45, No. 5, 753–759, 1997.
25. Wang, M. Y., J. Xu, J. Wu, Y. Yan, and H. L. Li, "FDTD study on scattering of metallic column covered by double-negative metamaterial," *Journal of Electromagnetic Wave Applications*, Vol. 21, No. 12, 1905–1914, 2007.
26. Hu, X. J. and D. B. Ge, "Study on conformal FDTD for electromagnetic scattering by targets with thin coating," *Progress In Electromagnetics Research*, PIER 79, 305–319, 2008.
27. Afrooz, K., A. Abdipour, A. Tavakoli, and M. Movahhedi, "Time domain analysis of active transmission line using FDTD technique (application to cicrowave/mm-wave transistors)," *Progress In Electromagnetics Research*, PIER 77, 309–328, 2007.
28. Berenger, J. P., "Three-dimensional perfectly matched layer for the absorption of electromagnetic waves," *J. Comput. Phys.*, Vol. 127, No. 2, 363–379, 1996.
29. Weber, M. J., *Handbook of Optical Materials*, CRC Press, New York, 2003.
30. Luebbers, R. J., F. Hunsberger, and K. S. Kunz, "A frequency-dependent finite-difference time-domain formulation fortransient propagation in plasma," *IEEE Trans. Antennas Propagat.*, Vol. 39, No. 1, 29–34, 1991.